JOC The Journal of Organic Chemistry

Article

pubs.acs.org/joc

Rh(III)-Catalyzed Cascade Oxidative Annulation of Benzoylacetonitrile with Alkynes: Computational Study of Mechanism, Reactivity, and Regioselectivity

Xiaoning Fu, Zhenfeng Shang, and Xiufang Xu*

Department of Chemistry, Key Laboratory of Advanced Energy Materials Chemistry (Ministry of Education), Nankai University, Tianjin 300071, P. R. China

Supporting Information

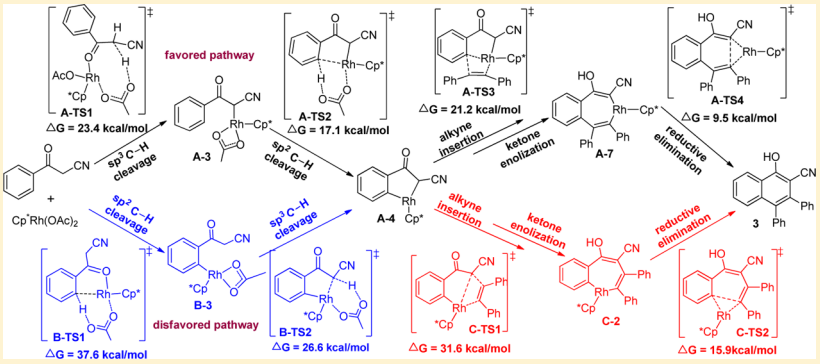

ABSTRACT: The mechanism of the rhodium-catalyzed cascade oxidative annulation of benzoylacetonitrile with alkynes is investigated using density functional theory calculations. The result shows that the reaction undergoes a stepwise annulation process, wherein the 1-naphthol acts as an intermediate. The first-step annulation involves the sp^3 C−H bond cleavage, sp^2 C−H bond cleavage, alkyne insertion into the Rh−C(sp^2) bond, ketone enolization, and reductive elimination to produce the 1-naphthol intermediate. The second-step annulation involves the O−H cleavage, sp^2 C−H bond cleavage, alkyne insertion into the Rh−C(sp^2) bond, and C−O reductive elimination to generate the final product naphtho[1,8-*bc*]-pyran. The sp^3 C−H bond cleavage rather than the sp^2 C−H bond cleavage is found to be the rate-determining step of the catalytic cycle. The ketone enolization should occur before the reductive elimination. The substituent effects on the reactivities and regioselectivities of reactions are also analyzed. These calculation results shed light on some ambiguous suggestions from experiments.

INTRODUCTION

Transition-metal-catalyzed C−H activation reactions[1] have attracted increasing interests in many fields of natural product synthesis, pharmaceutical chemistry, and material design.[2] For instances, the ruthenium-, rhodium-, and palladium-catalyzed oxidative couplings of aromatic substrates containing functional groups (e.g., ketones, aldehydes, carboxylic acids, and alcohols) with olefins, alkynes, or diazo esters provide efficient methods for the synthesis of substituted 5- or 6-membered heterocycles via formation of a C−C and a N−C or O−C bond.[3]

In contrast to facile routes of the sp^2 C−H functionalization, efficient strategies to achieve the sp^3 C−H activation are still limited due to the poor reactivity and the lack of regioselectivity. Therefore, the sp^3 C−H activation has recently attracted more attention. For instances, Curto and Kozlowski reported the Pd(II)-catalyzed selective activation of the benzylic and alkyl sp^3 C−H bonds rather than the arene sp^2 C−H bonds in order to achieve cross-dehydrogenative coupling (CDC) reactions.[4] Gaunt and co-workers developed a steric tethering approach to accomplish the sp^3 C−H activation of primary amino alcohols with a palladium catalyst.[5] Yu and co-workers scrutinized computationally and experimentally the mechanism of platinum(II)-catalyzed intramolecular cyclization of ortho-substituted aryl alkynes and compared three sp^3 C−H bond activation modes.[6] Taking amino acid as the transient directing group, Yu and co-workers developed a new method for sp^3 C−H activation.[7] However, reactions involving simultaneous dual functionalization of sp^3 C−H bond and sp^2 C−H bond have been rarely reported. In 2014, Zhang and co-workers developed a Rh(III)-catalyzed oxidative coupling reaction of naphthoquinones with alkynes to synthesize tetracyclic naphthoxazole derivatives, and they proposed that the reaction involved key steps of sp^2 C−H activation and sp^3 C−H cleavage/shift.[8] Recently, Zhou and co-workers developed the Rh(III)-catalyzed redox-neutral annulation reaction of 1-naphthylamine *N*-oxides with diazo compounds, which represented the first example of dual functionalization of unactivated primary sp^3 C−H and sp^2 C−H bonds with diazocarbonyl compounds. Their computational studies dis-

Received: June 30, 2016
Published: August 17, 2016

DOI: 10.1021/acs.joc.6b01567
J. Org. Chem. 2016, 81, 8378−8385

closed that the sp^2 C−H bond cleavage took place prior to the sp^3 C−H bond cleavage and the sp^3 C−H bond was activated by the free acetate in the reaction system.[9] Li and co-workers reported the DFT studies about rhodium-catalyzed sp^3 and sp^2 C−H activation of phenacyl ammonium salts and revealed that the sp^2 C−H activation occurred via a concerted metalation−deprotonation (CMD) mechanism. However, in their paper they did not elucidate the transition state and the activation energy for the sp^3 C−H activation step.[10]

Recently, Wang and co-workers reported the rhodium-catalyzed cascade oxidative annulation of benzoylacetonitrile with internal alkynes to give substituted naphtho[1,8-*bc*]pyrans by the sequential cleavage of sp^3 C−H/sp^2 C−H and sp^2 C−H/O−H bonds (Scheme 1).[11] These cascade reactions were

Scheme 1. Rhodium-Catalyzed Cascade Oxidative Annulation of Benzoylacetonitrile with Alkynes Studied Experimentally by Wang and Co-workers[11]

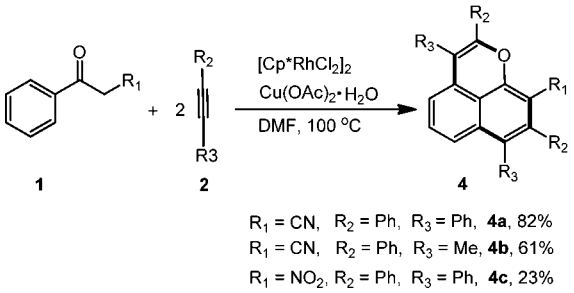

highly regioselective with unsymmetrical alkynes, and some of the naphtha[1,8-*bc*]pyran products responded to the intense fluorescence emission in the solid state. Significantly, these reactions provided new methods to synthesize substituted naphtho[1,8-*bc*]-pyrans from accessible starting materials.

In contrast to the wide variety of experimental studies, the computational studies on transition-metal catalyzed C−H activation reactions are still undeveloped and mainly focused on sp^2 C−H functionalization.[13] Experimental and computational studies by Guimond, Gorelsky, and Fagnou showed that the concerted metalation−deprotonation (CMD) was the turnover-limiting step in the Rh(III)-catalyzed (4 + 2) annulation of benzhydroxamic acid derivatives with acetylene (Scheme 2A).[12a] In these systems only one C−H bond was available for activation. While two selective sites for C−H activation were realized in the Rh(III)-catalyzed (4 + 2) annulations of pyridine and pyridine *N*-oxide substrates with alkyne,[14] and computational studies by Houk and co-workers revealed that the alkyne-insertion step was favored at C2 over C4, this preference was largely influenced by electrostatic interactions between the alkyne and the heteroarene (Scheme 2B).[12b] In the case of the Rh(III)-catalyzed cascade oxidative annulation of benzoylacetonitrile with internal alkynes (Scheme 1),[11] three sites for C−H cleavage were involved: one sp^3 C−H bond and two sp^2 C−H bonds (Scheme 2C).

Although Wang and co-workers proposed several reaction pathways and suggested that the cleavage of the sp^2 C−H bond of phenyl ring should be the rate-determining step,[11] the mechanism of the Rh(III)-catalyzed cascade oxidative annulation of benzoylacetonitrile with internal alkynes remains unclear. The major problems include the following: (1) What is the actual cleavage sequence of the sp^3 and sp^2 C−H bonds in this new reaction? (2) Does the alkyne prefer to insert into

Scheme 2. Rh(III)-Catalyzed (4 + 2) Annulation Studied Computationally (A) by Guimond, Gorelsky, and Fagnou, (B) by Houk and Co-workers, and (C) in This Work[12]

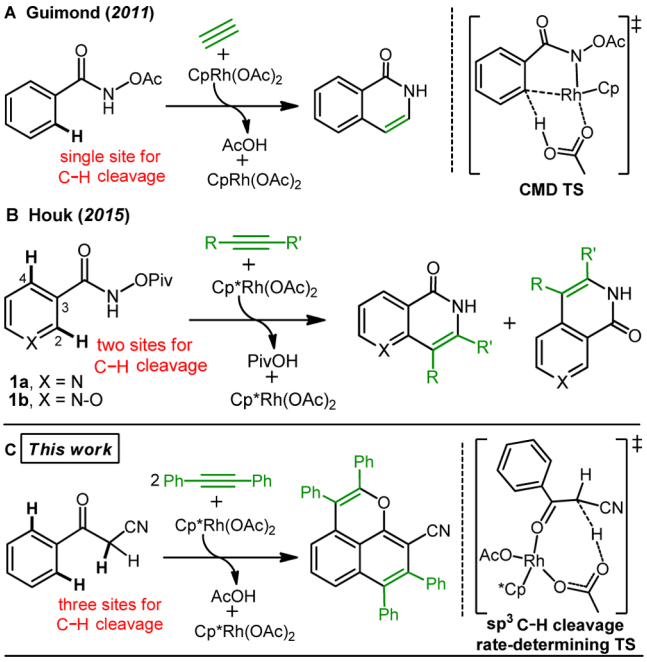

the Rh-alkyl (sp^3) bond or into the Rh-aryl (sp^2) bond? (3) What is the actual sequence of ketone enolization and reductive elimination of the seven-membered metallacycle intermediate in the first-step annulation? (4) Is it possible that the rate-determining step may be other step instead of the cleavage of the sp^2 C−H bond of the phenyl ring, like the case reported by Simmons and Hartwig?[15] Herein, we wish to report the DFT investigation on the actual rate-determining step, the order of cleavage of sp^3 and sp^2 C−H bonds, the preferred position of alkyne insertion, and the actual sequence of ketone enolization and reductive elimination for the rhodium-catalyzed cascade oxidative annulation of benzoylacetonitrile with alkynes. In addition, the substituent effect on the reactivities and regioselectivities of reactions are also discussed.

COMPUTATIONAL DETAILS

All of the calculations were carried out using the Gaussian 09 program.[16] Geometry optimization and frequency analysis were performed in *N*,*N*-dimethylformamide solvent with the SMD[17] solvation model using B3LYP functional[18] and a mixed basis set of SDD[19] for Rh and Cu and 6-311G(d) for other atoms. Intrinsic reaction coordinate (IRC)[20] calculations were conducted to determine the connectivity of minima and transition states. Single point energy calculations were carried out with the M06 functional,[21] a mixed basis set of SDD for Rh and Cu and 6-311+G(d,p) for other atoms, and the SMD solvation model with *N*,*N*-dimethylformamide as the solvent. Grimme's DFT-D3 dispersion corrections were calculated for the M06 functional with zero damping,[22] using the DFTD3 program.[23] Gibbs free energy values were the sum of the electronic energy from the single point calculations, the M06-D3 dispersion corrections, and the thermal corrections obtained by the frequency calculations. All of the Gibbs energies shown in this article were calculated at 1 atm and 373.15 K.

RESULTS AND DISCUSSION

The experimental results reported by Wang and co-workers indicated that, in the Rh(III)-catalyzed cascade oxidative

DOI: 10.1021/acs.joc.6b01567
J. Org. Chem. 2016, 81, 8378−8385

annulation of benzoylacetonitrile with alkynes, the double oxidative insertion of alkynes was a stepwise process, wherein the substituted 1-naphthol acted as an intermediate.[11] Here, we explore the potential energy surfaces for the proposed pathways of this reaction using density functional theory computations. As shown in Scheme 3a, the rhodium dimer $[Cp^*RhCl_2]_2$ as a

Scheme 3. Possible Mechanisms for (a) the First-Step Annulation of Benzoylacetonitrile and (b) the Second-Step Annulation of 1-Naphthol 3

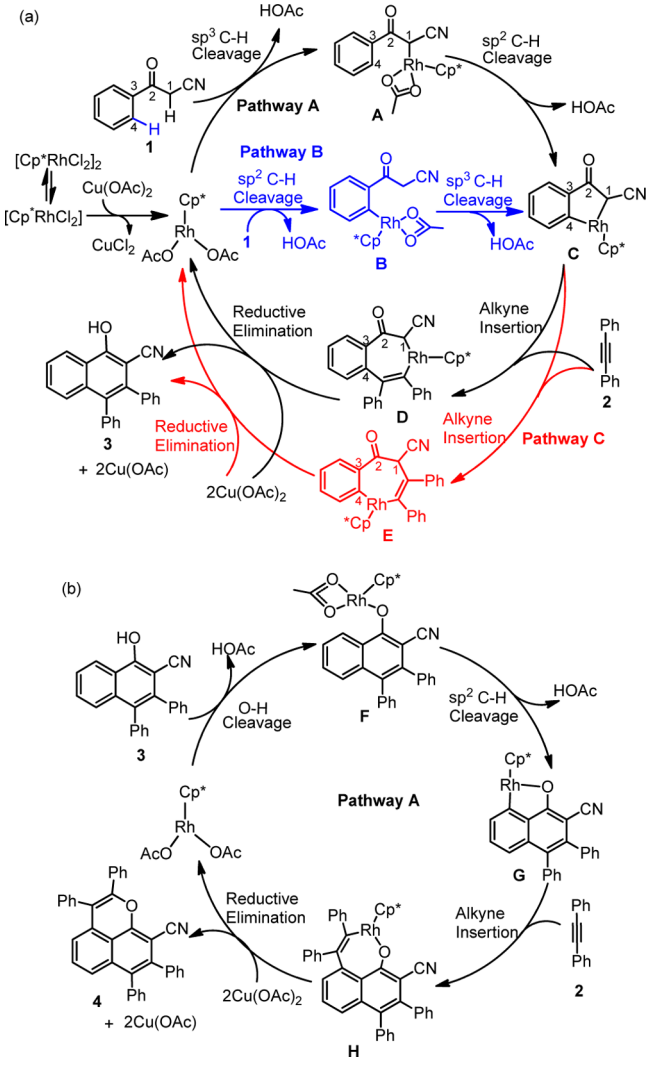

precatalyst initially dissociated into a coordinatively unsaturated monomer $[Cp^*RhCl_2]$, which subsequently formed a more stable species $[Cp^*Rh(OAc)_2]$ through the ligand exchange with acetates, and this process was totally exothermic by 8.5 kcal/mol. In addition, because $[Cp^*Rh(OAc)_2]$ was more stable than its dimer $[Cp^*Rh(OAc)_2]_2$ by 14.5 kcal/mol, $[Cp^*Rh(OAc)_2]$ should act as the active catalyst entering the catalytic cycle.

In the presence of the active catalyst $[Cp^*Rh(OAc)_2]$, the benzoylacetonitrile substrate would undergo a sequential cleavage of sp^3 C−H bond/sp^2 C−H bond (pathway A) or a sequential cleavage of sp^2 C−H bond/sp^3 C−H bond (pathway B) to produce the intermediate **C**. Subsequently, the alkyne might insert into the Rh−C4 (sp^2) bond to form the intermediate **D** or insert into the Rh−C1 (sp^3) bond to form the intermediate **E**. Then, the aromatization-driven reductive elimination of **C** or **D** could produce 1-naphthol **3** as the product of the first-step annulation. Alternatively, as will be illustrated in detail later (Figure 3), ketone enolization of **C** or **D** followed by reductive elimination may also produce 1-naphthol **3**.

The second-step annulation of 1-naphthol **3** involves a sequential O−H cleavage, sp^2 C−H cleavage, alkyne insertion, and reductive elimination to generate the final product naphtho[1,8-*bc*]pyran **4** (Scheme 3b). This mechanism was the same as that proposed by Ackermann and Miura and their co-workers.[24] However, to our best knowledge, detailed computational studies on the mechanism of Rh(III)-catalyzed annulation of 1-naphthol with alkyne have not been reported as yet.

sp^3/sp^2 C−H Activation Pathways for the Formation of the Five-Membered Metallacycle Intermediate. We first consider the possible pathways involving cleavage of sp^3/sp^2 C−H bonds for the formation of the five-membered metallacycle intermediate **C** (Scheme 3a). The computed Gibbs free energy profiles are shown in Figure 1.

Along pathway A (black line in Figure 1), the benzoylacetonitrile substrate **1** initially coordinated to the rhodium center of the active catalyst $[Cp^*Rh(OAc)_2]$ with the oxygen to form the intermediate **A-1**, in which both acetate ligands were monodentate. Moreover, the O−H bond between one H atom at the C1(sp^3) of substrate **1** and one O atom of the acetate ligand was formed. Then the cleavage of sp^3 C−H bond via the deprotonation with one of acetate ligands (**A-TS1**) and the subsequent release of HOAc afforded intermediate **A-2**. This step required an overall activation free energy of 23.4 kcal/mol (from **1** plus catalyst to **A-TS1**).The computational study by Yang, Houk, and Wu showed that the N−H deprotonation step in the rhodium(III)-catalyzed redox coupling reaction of *N*-phenoxyacetamides with alkynes occurred via a transition state similar to **TS1** with an energy barrier of 17.5 kcal/mol,[13d] indicating that the sp^3 C−H deprotonation of benzoylacetonitrile was more difficult to take place than the N−H deprotonation of *N*-phenoxyacetamide. In the following step, **A-2** isomerized to **A-3**, in which the substrate was bonded to the rhodium center with the Rh−C1(sp^3) bond and the remaining acetate ligand became bidentate. Next, **A-3** underwent a concerted metalation−deprotonation (CMD) process through the six-membered ring transition state **A-TS2**, in which the remaining acetate ligand acted as the base to deprotonate an ortho proton and the Rh metal center interacted strongly with both atoms of the breaking C4−H bond. In **A-TS2**, the O−H, C4−H, Rh−C4, and Rh−H distances were 1.27, 1.38, 2.25, and 2.28 Å, respectively (Figure 2, **A-TS2**), suggesting that the sp^2 C−H bond cleavage and Rh−C bond formation occurred simultaneously in the CMD process. This step overcame an energy barrier of 21.6 kcal/mol (from **A-3** to **A-TS2**).

In pathway B (blue line in Figure 1), the benzoylacetonitrile substrate coordinated to the active catalyst $[Cp^*Rh(OAc)_2]$ with the oxygen to afford the intermediate **B-1**, in which the O−H bond between the *ortho*-H atom of the phenyl ring and one O atom of the acetate ligand was formed. **B-1** was a bit more stable than **A-1** by 0.1 kcal/mol. The following sp^2 C−H bond cleavage occurred via a CMD mechanism with a high energy barrier of 37.6 kal/mol (**B-TS1**). Moreover, the subsequent transition state for the sp^3 C−H bond cleavage (**B-TS2**) was less stable than **A-TS2**. Thus, pathway A was the

DOI: 10.1021/acs.joc.6b01567
J. Org. Chem. 2016, 81, 8378−8385

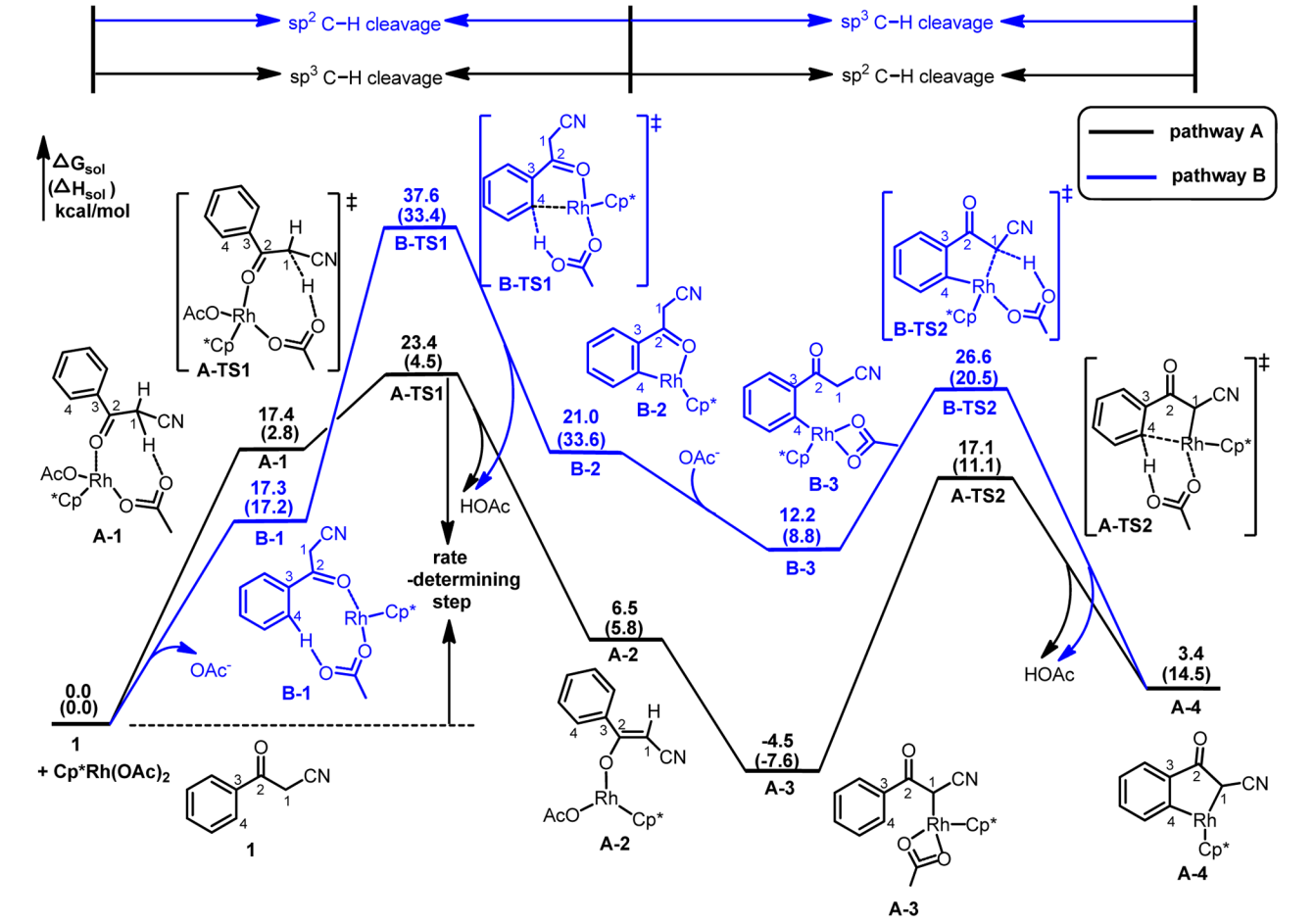

Figure 1. Energy profiles of the sp^3/sp^2 C−H activation pathways for the formation of the five-membered metallacycle intermediate **A-4**. ΔG_{sol} and ΔH_{sol} refer to the Gibbs free energy and enthalpy calculated with solvation model, respectively. All energies are with respect to substrate **1** and the active catalyst, Cp*Rh(OAc)$_2$.

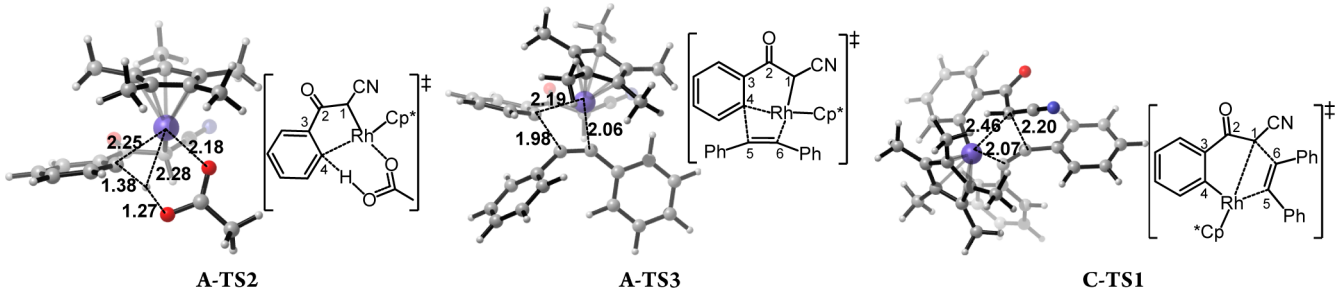

Figure 2. Geometric structures for selected transition states in the pathways. Distances are in angstroms.

preferred route, along which the benzoylacetonitrile substrate underwent the sequential cleavage of sp^3 C−H bond and sp^2 C−H bond to afford the five-membered metallacycle intermediate **A-4**.

Alkyne Insertion and Reductive Elimination Pathways for the Formation of 1-Naphthol 3. As shown in Figure 3, the coordination of phenyl-substituted alkyne to the rhodium center of **A-4** afforded the intermediate **A-5**. Subsequently, the alkyne insertion took place from the intermediate **A-5** via two distinct pathways: the alkyne may insert into the Rh−C4(sp^2) bond (**A-TS3**, Figure 2) to form the seven-membered metallacycle **A-6** (pathway A) or insert into the Rh−C1(sp^3) bond (**C-TS1**, Figure 2) to form an isomeric metallacycle **C-1** (pathway B). The computed activation barrier of the alkyne insertion into the Rh−C4(sp^2) bond (**A-TS3**) was 10.4 kcal/mol lower than that of the insertion into the Rh−C1(sp^3) bond (**C-TS1**). The higher activity of alkyne insertion into the Rh−C4(sp^2) bond was attributed to the greater orbital overlap of the HOMO of the metallacycle intermediate **A-4** and the LUMO of the alkyne. As illustrated in Figure 4, the HOMO-2 of **A-5** was mainly localized at the π orbital of the phenyl ring of substrate **1** and the coordinated alkyne bond. (The HOMO and HOMO-1 of **A-5**, respectively, corresponded to the d → π^* backdonation and π → d coordination between the rhodium center and the alkyne, respectively, which contributed to the formation of **A-5** from **A-4** and the alkyne; see Figure S1 in the Supporting Information.) Therefore, the attack of alkyne at the sp^2 carbon (C4) resulted in the favorable orbital overlap

DOI: 10.1021/acs.joc.6b01567
J. Org. Chem. 2016, 81, 8378−8385

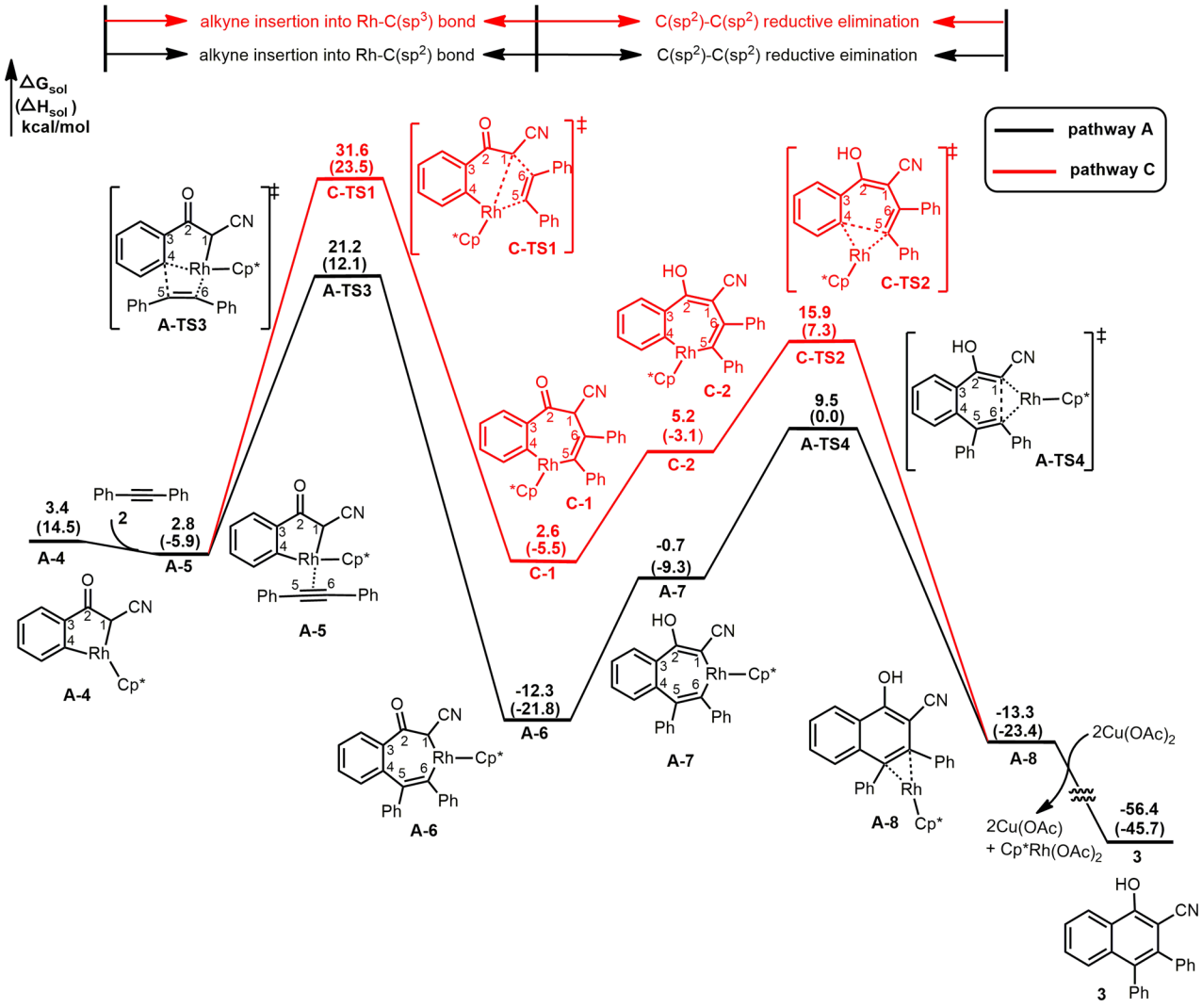

Figure 3. Energy profiles of the alkyne insertion and reductive elimination pathways. ΔG_{sol} and ΔH_{sol} refer to the Gibbs free energy and enthalpy calculated with solvation model, respectively. All energies are with respect to substrate **1** and the active catalyst, Cp*Rh(OAc)$_2$.

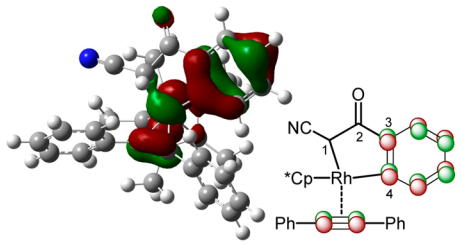

Figure 4. HOMO-2 of intermediate **A-5**.

between the phenyl ring π orbital and the alkyne π^* orbital. Thus, for the insertion of the first alkyne in the reaction, the first C−C bond was formed with the *ortho*-carbon (C4) of the phenyl ring. Similarly, computational studies by Gulías, Mascareñas, and co-workers disclosed that the alkyne inserted into the rhodium−C(sp^2) bond of the rhodacycle intermediate in the rhodium(III)-catalyzed intermolecular annulations of acrylamides and alkynes.[13a] Moreover, their studies also revealed that the alkyne inserted into the rhodium−nitrogen bond in the rhodium(III)-catalyzed intramolecular annulations of acrylamides bearing N-tethered alkynes.

The metallacycle intermediate **A-6** subsequently underwent the enolization to form the intermediate **A-7**. Then **A-7** underwent C(sp^2)−C(sp^2) reductive elimination to form the second new C−C bond via the transition state **A-TS4**, leading to complex **A-8**. This step required a free energy barrier of 21.8 kcal/mol (from **A-6** to **A-TS4**). Finally, **A-8** released the first-step product, 1-naphthol **3**, and Rh(I) was simultaneously reoxidated to Rh(III) by Cu(OAc)$_2$. Although pathway C required a low barrier for the reductive elimination between two sp^2 carbons (**C-1** → **C-TS2**, $\Delta G^{\ddagger}$ = 13.3 kcal/mol), the high barrier of alkyne insertion (**A-5** → **C-TS1**, $\Delta G^{\ddagger}$ = 28.8 kcal/mol) ruled out the possibility of this pathway in the preferred catalytic cycle.

We also considered the possibility of the direct reductive elimination of **A-6** and **C-1** before they underwent the ketone enolization. The computed results (Figure 5a) indicated that the activation free energy of the direct C(sp^3)−C(sp^2) reductive elimination of **A-6** via the transition state **A-TS4′** is 6.3 kcal/mol higher than that of the C(sp^2)−C(sp^2) reductive elimination via the transition state **A-TS4**. This is because the transition state **A-TS4**, which has a C1═C2 double bond in the forming six-membered ring, is more highly π-conjugative than the transition state **A-TS4′**, which has a C1−C2 single bond in

DOI: 10.1021/acs.joc.6b01567
J. Org. Chem. 2016, 81, 8378−8385

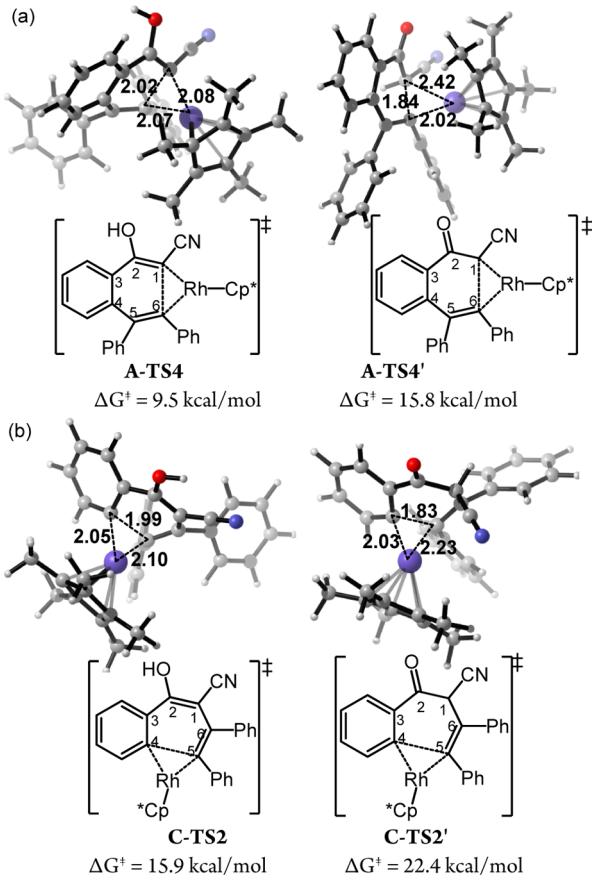

Figure 5. Transition states in two possible pathways for (a) the reductive elimination of **A-6** and (b) the reductive elimination of **C-1**.

the forming six-membered ring. Moreover, the high π-conjugative structure of the forming six-membered ring in **A-TS4** can facilitate the reductive elimination step by the developing ligand π-Rh coordination.[25] In addition, our computational results indicate that 1-naphthol **3**, the product of the reductive elimination via **A-TS4**, is more stable than the keto-form isomer **3′** by 11.9 kcal/mol, which should be attributed to the more highly π-conjugative structure in **3** than in **3′** (Figure S2 in the Supporting Information). Similarly, the activation free energy of the direct reductive elimination of **C-1** via the transition state **C-TS2′** is 6.5 kcal/mol higher than that of the reductive elimination via **C-TS2** (Figure 5b). These results indicated that the ketone enolization of **A-6** (or **C-1**) should occur before the reductive elimination step.

Pathways for the Second-Step Annulation of 1-Naphthol 3 to Generate the Final Naphtho[1,8-*bc*]pyran Product 4. Pathways for the second-step annulation of 1-naphthol **3** with the other alkyne to generate the final product naphtho[1,8-*bc*]pyran **4** were also calculated, and the energy profiles were shown in Figure 6.

First, the deprotonation of phenolic hydrogen by one of the acetate ligands of the catalyst led to the intermediate **A-10**, in which the phenolic oxygen coordinated to the Rh center and the remaining acetate ligand became bidentate. Then **A-10** underwent a CMD process through the six-membered ring transition state **A-TS5.** The remaining acetate ligand acted as the base to deprotonate a benzene-ring proton and the Rh center interacted strongly with both atoms of the breaking C−H bond, leading to the intermediate **A-11** with the release of HOAc. This step had an energy barrier of 20.8 kcal/mol. Subsequently, the alkyne insertion into the Rh−C(sp^2) bond took place to afford the metallacycle intermediate **A-13** with an energy barrier of 17.0 kcal/mol. Then the reductive elimination of **A-13** via the transition state **A-TS7** produced the product complex **A-14**. This step required an activation free energy of 21.5 kcal/mol. It was noteworthy that, although it was the highest energy barrier in the second-step annulation, it was still lower than the highest energy barrier of the sp^3 C−H bond cleavage of the first-step annulation. Finally, **A-14** released the final product, naphtho[1,8-*bc*]pyran **4**, and Rh(I) was simultaneously reoxidated to Rh(III) by $Cu(OAc)_2$.

In summary, the preferred catalytic cycle of Rh(III)-catalyzed cascade oxidative annulation of benzoylacetonitrile with internal alkynes involved a stepwise annulation, wherein the

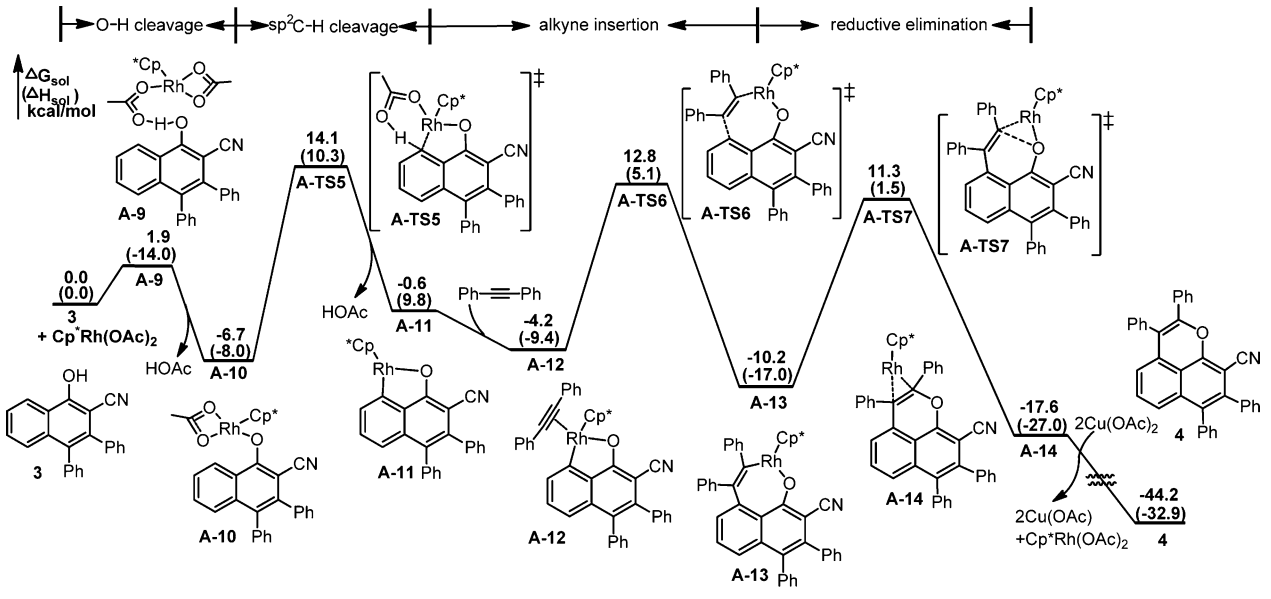

Figure 6. Energy profile of the second-step annulation of 1-naphthol **3** with alkyne. ΔG_{sol} and ΔH_{sol} refer to the Gibbs free energy and enthalpy calculated with solvation model, respectively. All energies are with respect to 1-naphthol **3** and the active catalyst, $Cp^*Rh(OAc)_2$.

DOI: 10.1021/acs.joc.6b01567
J. Org. Chem. 2016, 81, 8378−8385

substituted 1-naphthol acted as an intermediate. The first-step annulation involved five key steps: sp^3 C−H bond cleavage, sp^2 C−H bond cleavage, alkyne insertion into the Rh−C(sp^2) bond, ketone enolization of the seven-membered metallacycle intermediate, and C(sp^2)−C(sp^2) reductive elimination to produce the 1-naphthol intermediate (pathway A, shown in black in Figures 1 and 3). The second-step annulation involved four key steps: O−H cleavage, sp^2 C−H bond cleavage, alkyne insertion into the Rh−C(sp^2) bond, and C−O reductive elimination to generate the final product naphtho[1,8-*bc*]-pyran. The sp^3 C−H bond cleavage of the first-step annulation was suggested to be the rate-determining step of the catalytic cycle because it had the highest energy barrier.

Origins of the Substituent Effect on Reactivities and Regioselectivities. Experimental observations have indicated that the cyano group (CN) at the C1 position of substrate **1** promoted the reaction and resulted in the higher yield (82%), while the nitro group (NO_2) at the C1 position of substrate **1** led to a lower yield (23%) (Scheme 1).[11] The above mechanism study showed that the sp^3 C−H bond cleavage was the rate-determining step. Obviously, the substituents at the C1 position of substrate **1** had a great effect on the activation energy of the rate-determining step, thus leading to the distinct reactivities. To analyze the origins of substituent effects on reactivities, we further computed the activation energy of the rate-determining step with 2-nitro-1-phenylethanone. As shown in Figure 7, a good agreement with the experimental reactivities was obtained: the activation energy of the rate-determining step with 2-nitro-1-phenylethanone ($\Delta G^{\ddagger}$ = 24.2 kcal/mol) was 0.8 kcal/mol higher than that with benzoylacetonitrile, which consequently resulted in a relatively lower reactivity with 2-nitro-1-phenylethanone than with benzoylacetonitrile.

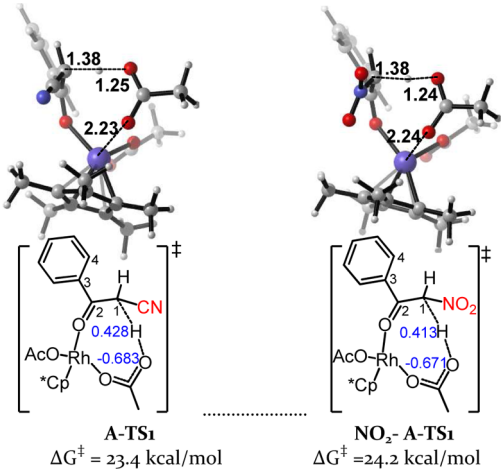

Figure 7. Free energies of activation and natural population analysis (NPA) charges of the transition states for the rate-determining sp^3 C−H bond cleavage with different substrates. Numbers in black are bond lengths in Å, and numbers in blue are NPA charges.

NPA charges[26] for the two transition states are also shown in Figure 7 (numbers in blue). Although NO_2 and CN were both electron-withdrawing groups, the conjugative effect of NO_2 group led to a less-positive NPA charge on the leaving hydrogen at the C1 position in **NO_2-A-TS1**. Therefore, the leaving hydrogen was more difficult to be taken away by the electrostatic interaction with the acetate ligand in the reaction with 2-nitro-1-phenylethanone.

To explore why the unsymmetrical alkyne 1-phenyl-1-propyne gave the single regioisomeric product **4b**, in which the methyl group of the alkyne was positioned proximal to the phenyl group of benzoylacetonitrile substrate (Scheme. 1),[11] we computed the activation energy barriers of two alkyne insertion pathways with 1-phenyl-1-propyne. As shown in Figure 8, the transition state **TS3-*proximal*** was 1.7 kcal/mol lower in energy than the transition state **TS3-*distal***, thus leading to the single regioisomeric product **4b**. NPA charge analysis (Figure 8) showed that the C4 atom in the five-membered metallacycle intermediate **A-4** was negatively charged. On the other hand, in 1-phenyl-1-propyne (**2′**) the C5 atom bearing the methyl group was positively charged while the C6 atom bearing the phenyl group was negatively charged. The electrostatic interactions between the C4 atom of **A-4** and the C5 atom of 1-phenyl-1-propyne were stronger than that between the C4 atom and the C6 atom. Therefore, the insertion of C5 rather than the insertion of C6 into the Rh−C4 bond was favored. Moreover, among **TS3-*proximal*** and **TS3-*distal***, the C4 atom was more negatively charged and the C5 atom was more positively charged in **TS3-*proximal***, which resulted in the stronger electrostatic interactions between C4 and C5 in **TS3-*proximal*** than in **TS3-*distal***. Thus, **TS3-*proximal*** was more stable than **TS3-*distal***.

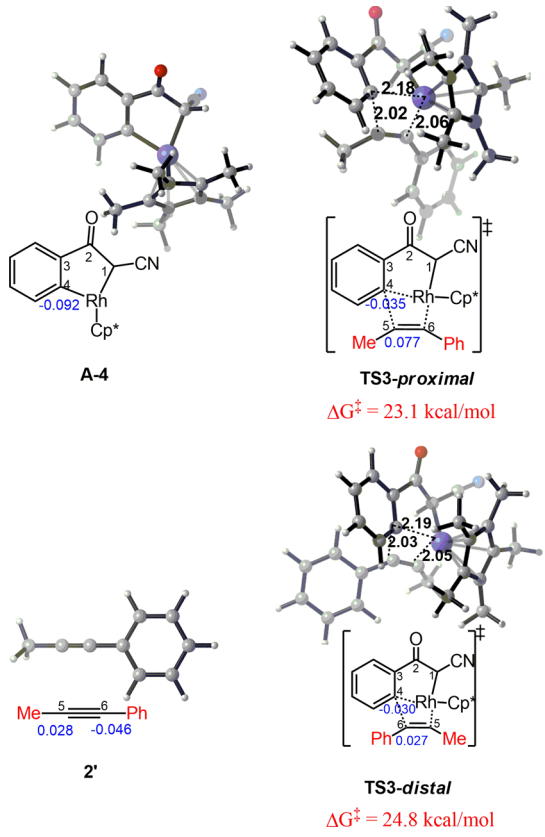

Figure 8. Free energies of activation and natural population analysis (NPA) charges of the transition states for the two alkyne-insertion pathways with 1-phenyl-1-propyne. Numbers in black are bond lengths in Å, and numbers in blue are NPA charges.

DOI: 10.1021/acs.joc.6b01567
J. Org. Chem. 2016, 81, 8378−8385

CONCLUSION

In summary, we performed DFT calculations to explore the detailed mechanism, reactivity, and regioselectivity in the rhodium-catalyzed cascade oxidative annulation of benzoylacetonitrile with alkynes. The first-step annulation involved sp^3 C−H bond cleavage, sp^2 C−H bond cleavage, alkyne insertion into the Rh−C(sp^2) bond, ketone enolization, and C(sp^2)−C(sp^2) reductive elimination to produce the 1-naphthol intermediate. The second-step annulation involved O−H cleavage, sp^2 C−H bond cleavage, alkyne insertion into the Rh−C(sp^2) bond, and C−O reductive elimination to generate the final product naphtho[1,8-*bc*]-pyran. The product regioselectivity was exhibited during the formation of the first C−C bond in the alkyne-insertion step due to the difference in electrostatic interactions from the different orientations of the alkyne substituent. Our calculation suggested that the ketone enolization should occur before the reductive elimination. The actual rate-determining step was the sp^3 C−H bond cleavage for the first-step annulation, which was consistent with the effect of substituent at C1 of substrate **1** on the reactivity. The mechanism disclosed here may have broad implications in the understanding and development of transition metal-catalyzed C−H activation reactions.

ASSOCIATED CONTENT

Supporting Information

The Supporting Information is available free of charge on the ACS Publications website at DOI: 10.1021/acs.joc.6b01567.

Complete reference of Gaussian 09, as well as optimized geometries and energies of all computed species (PDF)

AUTHOR INFORMATION

Corresponding Author

*E-mail: xxfang@nankai.edu.cn.

Notes

The authors declare no competing financial interest.

ACKNOWLEDGMENTS

We are grateful to the Natural Science Foundation of China (Project 21421001) and MOE Innovation Teams (IRT-13R30 and IRT13022) of China for the financial support of this research. We are indebted to Professor Baiquan Wang for his helpful discussions and Professor Zunsheng Cai for his linguistic fixing.

REFERENCES

(1) (a) Ackermann, L. *Acc. Chem. Res.* **2014**, *47*, 281. (b) Wencel-Delord, J.; Droege, T.; Liu, F.; Glorius, F. *Chem. Soc. Rev.* **2011**, *40*, 4740. (c) Kakiuchi, F.; Kochi, T. *Synthesis* **2008**, *2008*, 3013. (d) Ackermann, L. *Chem. Rev.* **2011**, *111*, 1315.

(2) (a) Chiba, S.; Chen, H. *Org. Biomol. Chem.* **2014**, *12*, 4051. (b) Wencel-Delord, J.; Glorius, F. *Nat. Chem.* **2013**, *5*, 369. (c) Rouquet, G.; Chatani, N. *Angew. Chem., Int. Ed.* **2013**, *52*, 11726. (d) Okamoto, K.; Zhang, J.; Housekeeper, J. B.; Marder, S. R.; Luscombe, C. K. *Macromolecules* **2013**, *46*, 8059. (e) Yamaguchi, J.; Yamaguchi, A. D.; Itami, K. *Angew. Chem., Int. Ed.* **2012**, *51*, 8960. (f) Chen, D. Y. K.; Youn, S. W. *Chem. - Eur. J.* **2012**, *18*, 9452. (g) Gutekunst, W. R.; Baran, P. S. *Chem. Soc. Rev.* **2011**, *40*, 1976.

(3) (a) Zhong, H.; Yang, D.; Wang, S.; Huang, J. *Chem. Commun.* **2012**, *48*, 3236. (b) Rakshit, S.; Patureau, F. W.; Glorius, F. *J. Am. Chem. Soc.* **2010**, *132*, 9585. (c) Stuart, D. R.; Alsabeh, P.; Kuhn, M.; Fagnou, K. *J. Am. Chem. Soc.* **2010**, *132*, 18326. (d) Xu, L.; Zhu, Q.; Huang, G.; Cheng, B.; Xia, Y. *J. Org. Chem.* **2012**, *77*, 3017. (e) Chinnagolla, R. K.; Jeganmohan, M. *Chem. Commun.* **2012**, *48*, 2030. (f) Chinnagolla, R. K.; Jeganmohan, M. *Eur. J. Org. Chem.* **2012**, *2012*, 417. (g) Li, B.; Ma, J.; Wang, N.; Feng, H.; Xu, S.; Wang, B. *Org. Lett.* **2012**, *14*, 736. (h) Nakanowatari, S.; Ackermann, L. *Chem. - Eur. J.* **2015**, *21*, 16246.

(4) Curto, J. M.; Kozlowski, M. C. *J. Am. Chem. Soc.* **2015**, *137*, 18.

(5) Calleja, J.; Pla, D.; Gorman, T. W.; Domingo, V.; Haffemayer, B.; Gaunt, M. J. *Nat. Chem.* **2015**, *7*, 1009.

(6) Wang, Y.; Liao, W.; Huang, G.; Xia, Y.; Yu, Z. X. *J. Org. Chem.* **2014**, *79*, 5684.

(7) Zhang, F.-L.; Hong, K.; Li, T.-J.; Park, H.; Yu, J.-Q. *Science* **2016**, *351*, 252.

(8) Wang, M.; Zhang, C.; Sun, L. P.; Ding, C.; Zhang, A. *J. Org. Chem.* **2014**, *79*, 4553.

(9) Zhou, B.; Chen, Z.; Yang, Y.; Ai, W.; Tang, H.; Wu, Y.; Zhu, W.; Li, Y. *Angew. Chem., Int. Ed.* **2015**, *54*, 12121.

(10) Yu, S.; Liu, S.; Lan, Y.; Wan, B.; Li, X. *J. Am. Chem. Soc.* **2015**, *137*, 1623.

(11) Tan, X.; Liu, B.; Li, X.; Li, B.; Xu, S.; Song, H.; Wang, B. *J. Am. Chem. Soc.* **2012**, *134*, 16163.

(12) (a) Guimond, N.; Gorelsky, S. I.; Fagnou, K. *J. Am. Chem. Soc.* **2011**, *133*, 6449. (b) Neufeldt, S. R.; Jimenez-Oses, G.; Huckins, J. R.; Thiel, O. R.; Houk, K. N. *J. Am. Chem. Soc.* **2015**, *137*, 9843.

(13) (a) Quiñones, N.; Seoane, A.; García-Fandiño, R.; Mascareñas, J. L.; Gulías, M. *Chem. Sci.* **2013**, *4*, 2874. (b) Sperger, T.; Sanhueza, I. A.; Kalvet, I.; Schoenebeck, F. *Chem. Rev.* **2015**, *115*, 9532. (c) Zhang, M.; Huang, G. *Chem. - Eur. J.* **2016**, *22*, 9356. (d) Yang, Y. F.; Houk, K. N.; Wu, Y. D. *J. Am. Chem. Soc.* **2016**, *138*, 6861.

(14) Huckins, J. R.; Bercot, E. A.; Thiel, O. R.; Hwang, T. L.; Bio, M. M. *J. Am. Chem. Soc.* **2013**, *135*, 14492.

(15) Simmons, E. M.; Hartwig, J. F. *Angew. Chem., Int. Ed.* **2012**, *51*, 3066.

(16) Frisch, M. J.; et al. *Gaussian 09, Revision E.01*; Gaussian, Inc.: Wallingford, CT, 2013.

(17) Marenich, A. V.; Cramer, C. J.; Truhlar, D. G. *J. Phys. Chem. B* **2009**, *113*, 6378.

(18) (a) Becke, A. D. *J. Chem. Phys.* **1993**, *98*, 5648. (b) Raghavachari, K. *Theor. Chem. Acc.* **2000**, *103*, 361. (c) Becke, A. D. *J. Chem. Phys.* **1993**, *98*, 1372. (d) Lee, C.; Yang, W.; Parr, R. G. *Phys. Rev. B: Condens. Matter Mater. Phys.* **1988**, *37*, 785.

(19) Andrae, D.; Häussermann, U.; Dolg, M.; Stoll, H.; Preuss, H. *Theor. Chem. Acc.* **1990**, *77*, 123.

(20) Fukui, K. *Acc. Chem. Res.* **1981**, *14*, 363.

(21) Zhao, Y.; Truhlar, D. G. *J. Chem. Phys.* **2006**, *125*, 194101.

(22) Grimme, S.; Antony, J.; Ehrlich, S.; Krieg, H. *J. Chem. Phys.* **2010**, *132*, 154104.

(23) Grimme, S. *DFTD3, V2.0 Rev. 1*; University Münster: Münster, Germany, 2010.

(24) (a) Thirunavukkarasu, V. S.; Donati, M.; Ackermann, L. *Org. Lett.* **2012**, *14*, 3416. (b) Mochida, S.; Shimizu, M.; Hirano, K.; Satoh, T.; Miura, M. *Chem. - Asian J.* **2010**, *5*, 847.

(25) (a) Zuidema, E.; van Leeuwen, P. W. N. M.; Bo, C. *Organometallics* **2005**, *24*, 3703. (b) Yu, Z.-X.; Cheong, P. H.-Y.; Liu, P.; Legault, C. Y.; Wender, P. A.; Houk, K. N. *J. Am. Chem. Soc.* **2008**, *130*, 2378.

(26) Reed, A. E.; Weinstock, R. B.; Weinhold, F. *J. Chem. Phys.* **1985**, *83*, 735.

DOI: 10.1021/acs.joc.6b01567
J. Org. Chem. 2016, 81, 8378−8385